Electroreduction of CO_2 to ethanol by electrochemically deposited Cu-lignin complexes on Ni foam electrodes

Chanda, Debabrata; Tufa, Ramato Ashu; Aili, David; Basu, Suddhasatwa

Published in:
Nanotechnology

Link to article, DOI:
10.1088/1361-6528/ac302b

Publication date:
2022

Document Version
Peer reviewed version

Electroreduction of CO2 to ethanol by electrochemically deposited Cu-lignin complexes on Ni foam electrodes

Electroreduction of CO_2 to Ethanol by Electrochemically Deposited Cu-lignin Complexes on Ni foam Electrodes

Debabrata Chanda[1], Ramatu Ashu Tufa[2], David Aili[2], Suddhasatwa Basu[1,3]*

[1]Department of Chemical Engineering, Indian Institute of Technology Delhi, New Delhi 110016, India.
[2] Department of Energy Conversion and Storage, Technical University of Denmark, Elektrovej 375, 2800 Kgs Lyngby, Denmark
[3] CSIR-Institute of Minerals and Materials Technology, Bhubaneswar 751013, India

Table of Content

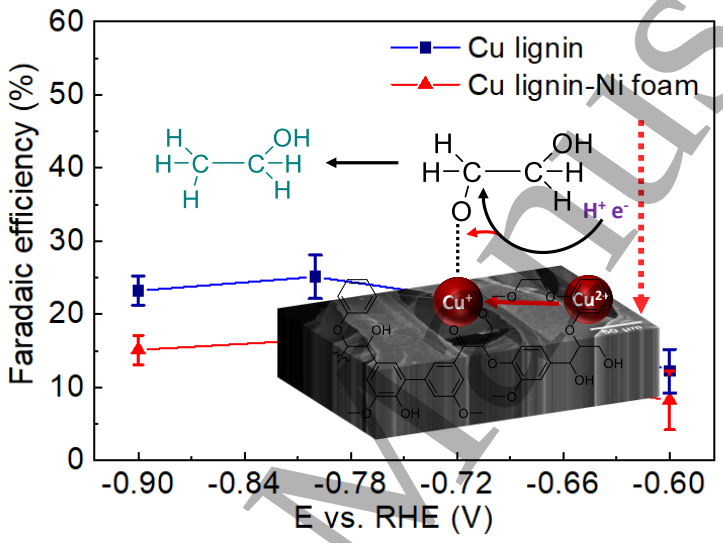

Abstract

A low cost, non-toxic and highly selective catalyst based on a Cu-lignin molecular complex is developed for CO_2 electroreduction to ethanol. Ni foam (NF), Cu-Ni foam (Cu-NF) and Cu-lignin-Ni foam (Cu-lignin-NF) were prepared by a facile and reproducible electrochemical deposition method. The electrochemical CO_2 reduction activity of Cu-lignin-NF was found to be higher than Cu-NF. A maximum faradaic efficiency of 23.2 % with current density of 22.5 mA cm^{-2} was obtained for Cu-lignin-NF at -0.80 V (vs. RHE) in 0.1 M Na_2SO_4 towards ethanol production. The enhancement of catalytic performance is attributed to the growth of the number of active sites and the change of oxidation states of Cu and NF due to the presence of lignin.

Keywords: CO_2 electroreduction, Cu-lignin complex, electrocatalyst, selectivity

Introduction

An increase in energy demands have stimulated intense research on alternative energy conversion systems with high efficiency, low cost, and low carbon emission [1-2]. Electrical energy conversion from renewable and intermittent energy sources, such as wind and solar, into chemical fuels by using electrochemical CO_2 reduction is an attractive concept to convert emitted CO_2 back to fuels. Electrochemical reduction of CO_2 allows for the conversion of a variety of value-added products such as carbon monoxide, formic acid, oxalic acid, methane, methanol, and ethanol [3-6]. Among these products, ethanol (a C_2 product) has been considered a particularly attractive product because of its high heating value (1366.8 kJ mol^{-1}) and commercial importance as a starting point of many processess substituting petrochemical routes. However, selective conversion of CO_2 into C_2 products still remains a challenge. C1 products like CO and formic acid (or formate) are often the favored CO_2 reduction products, since the reaction follows a less complex reaction pathway that involves one or two electron transfer processes [7-9]. Occasionally, methanol and methane have been found as a minor product during CO or formic acid formation [10-13]. C_2 products are generally less effectively formed than C_1 products, because the reaction pathway is more complex and involves more sequential mechaistivc steps. It is a primary challenge for the researchers to find out highly active and selective electrocatalysts to increase the reaction kinetics of ethanol production.

Copper-based catalysts have been widely used for the reduction of CO_2 to multicarbon mixed products. Cu based materials are good choices for CO_2 reduction as their selectively can be tailored by modification of the Cu surface with foreign d-group metals, different faceting and morphology and complexation [27-28]. The different Cu based catalysts tested for the

conversion of CO_2 to ethanol include metallic Cu [14-15], Cu nanoparticles [16-17], Cu_2O [18-20], Cu foam [21] and Cu salts [22-24]. Ren et al. [27] reported the possibility of selective electroreduction of CO_2 to ethanol with a maximum faradaic efficiency (FE) of 29 % by using Cu-based oxide catalysts surface-modified with with Zn as a cocatalyst. However, the Cu/Zn catalysts gave only low conversion selectivity and poor yield. Weng et al. [28] developed a new Cu-porphyrin complex structure, which efficiently catalyzed CO_2 reduction to C_2 products (methane and ethylene) in aqueous media. The oxidation state of the Cu and the built-in hydroxyl groups modified porphyrin ligand contributed a promising electrocatalytic performance [28]. On the other hand, Ni-based catalysts have shown to efficiently catalyze (up to 40% FE) the conversion of CO_2 to C_2 products at the small potential range [29-30]. However, the activity and selectivity of these catalysts was not sufficient due to their limited accessible active sites, requiring further exploration of new, high performance electrocatalysts.

In this regard, our primary target in the present work is to design a more selective Cu-based electrocatalyst for effective implementation of CO_2 electroreduction to ethanol on the surface of a catalyst via the following half-reaction [25]:

$$2CO_2 + 9H_2O + 12e^- \rightarrow C_2H_5OH + 12OH^- \quad (1)$$

The equilibrium potential (E^0) of the above reaction against SHE is 0.084 V. The selective reduction of CO_2 to ethanol on the Cu surface is rather complicated due to the multi-oriented reaction ability of CO which is the primary product of CO_2 reduction process [26]. The transformation of CO_2 to ethanol has been demonstrated by density functional theory (DFT), where the obtained pathway as follows [26].

This work present a new approach to CO_2 reduction, using a Cu-lignin decorated Ni foam (NF) electrode. Lignin is a biopolymer and contains a high amount of phenolic groups which can be connected with Cu and Fe centers to form the metal-lignin complex [31-32]. Its molecular structure is shown in Fig. 1. The new catalyst, was synthesized and the catalytic performance was evaluated based on the stability and selectivity towards electrochemical CO_2 reduction to ethanol, demonstrating excellent activity towards the reduction of CO_2 to ethanol compared to that of Cu decorated NF catalyst. The study paves the way for further investigation on non-noble transition metal complexes for electrochemical CO_2 reduction.

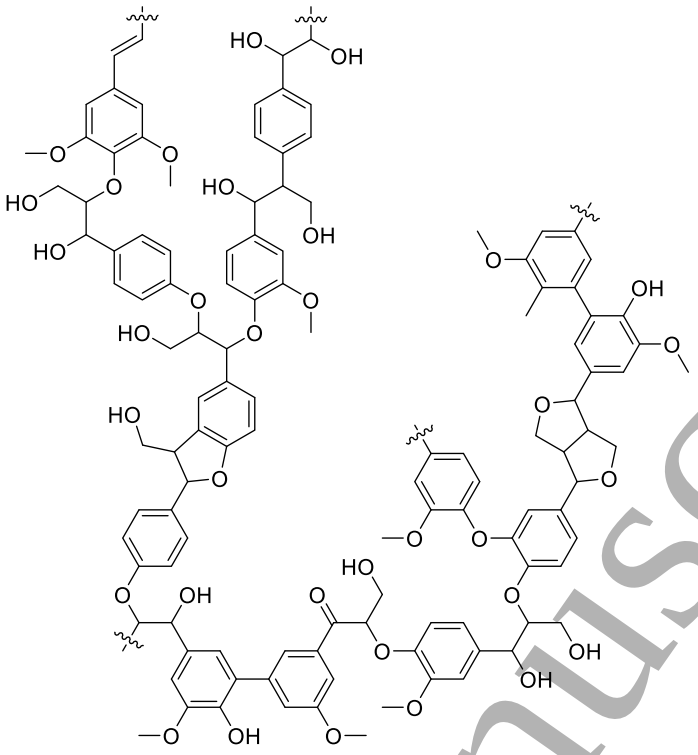

Figure 1. Molecular structure of lignin.

2. Materials and Methods

2.1 Materials

Copper (II) chloride ($CuCl_2$, Sigma aldrich, 98 %), lignin (alkaline, TCI, L0082), sodium sulfate (Na_2SO_4, Alpha chemical, 98 %), Nafion117® (Dupont, USA), Ni foam (Fiaxell, Switzerland) were used as received without further treatment. All experiments were carried out using ultra-pure 18 MΩ cm.

2.2. Catalyst and electrode layer Preparation

The conductive nickel foam (NF) substrates (0.34 cm × 1.9 cm in a rectangular shape, 0.5 mm thickness) were used for preparing Cu-lignin/NF catalysts. Two catalysts (Cu and Cu-lignin) were deposited on NF through the electrochemical deposition technique. For Cu-lignin preparation, 25 mg of lignin and 170 mg of $CuCl_2$ were dissolved in 25 mL deionized water with continuous stirring until a homogeneous solution was obtained. The electrochemical deposition was performed in a standard two-electrode glass cell at 22 °C. NF was used as the cathode, and a Pt rod served as the anode. The distance between the two electrodes was kept at 1 cm. The Cu-lignin deposition (3.5 mg cm^{-2} Cu loading) was carried out by applying a constant voltage of -2 V for 30 min between the electrodes. A similar method was adopted without using lignin for deposition of the Cu catalyst on NF. After deposition, the catalyst coated NF electrode was washed several times with ethanol and water to remove excess materials not

adhereing to the NF substrate, and then dried under vacuum at 60 °C for 1 h. Before the electrochemical CO_2 reduction test, 50 μL of 5 % Nafion® dispersion was homogeneously spread over the Cu-lignin catalyst coated NF electrodes and heated at 120 °C to prevent the mechanical loss of catalysts during the operation.

2.3. Physical characterization

The morphology of the prepared electrodes was characterized using a scanning electron microscope (SEM) (JEOL JSM 6010, Japan). The elemental composition of the prepared materials was determined by energy-dispersive X-ray spectroscopy (EDX) (Jeol 6010+, Japan). Structural characteristics of the catalysts were obtained by Rigaku Miniflex 600 X-ray diffractometer (Japan) using nickel filtered Cu-Kα radiation operated at 40 kV and 40 mA. The average wavelength of the radiation was 1.5425 Å. Diffractograms were taken between 2θ = 10°-80° using a step size of 0.033° [2θ] at a scan rate of 6° [2θ] min^{-1}. The high resolution transmission electron microscope (HRTEM) imaging was performed on a JEOL JEM-3010 (Japan) field-emission transmission electron microscope with an accelerating voltage of 200 kV. Raman spectroscopic measurements were carried out using a dispersive Raman microscope (Senterra R200-L, Bruker Optics, USA) with an excitation wavelength of 514 nm. UV-Vis measurements were performed by an Avaspec 2048 UV-Vis spectrophotometer with the sample prepared in DMSO/water (1:9) mixture. Fourier transform infrared spectroscopy (FTIR) was performed by using Nicolet 600 IR spectroscopy. X-ray photoelectron spectroscopy (XPS) of the catalyst samples were recorded using an ESCAProbeP (PHI 5000 Versa Probe II, FEI Inc) electron spectrometer with monochromatic Al Kα source (5.5 mA, 15 kV). For IR, SEM, UV-Vis, XRD, Raman, XPS and TEM analysis, the powders of the catalysts were obtained from the NF surface removed by scratching. The Cu dissolution in electrolyte was determined by an ICP-MS (Agilent Technologies, 7500 CE, USA). The CHNS analyzer (Elementar Vario Macro Cube) was used to determine the content of carbon and hydrogen. The obtained liquid products were quantified by Bruker Advance III 400 MHz NMR spectroscopy. Each ^{1}H-NMR sample contained of 325 μL sample solution, 65 μL of D_2O (deuterated water), and 30 μL of 10 mM DMSO as an internal standard. The gaseous products were identified and quantified by Nucon 5765 gas chromatograph.

The faradaic efficiency (FE) of ethanol production is estimated from the total amount of charge Q (coulomb) passed through the CO_2 saturated 0.1 M Na_2SO_4 electrolyte and consequently, the total amount of ethanol in moles ($n_{ethanol}$) produced. The ethanol

concentration in the electrolyte solution was measuremd using ^{1}H NMR spectroscopy with DMSO as an internal standard. The FE for ethanol can be expressed as:

$$FE = 12F \times n_{ethanol}/Q = 12F \times n_{ethanol}/(I \times t) \quad (2)$$

where, 12 is the no of electron transfer for ethanol production, I is the current at constant applied potential, F is the faradaic constant and t is the time period at a given applied potential. Similar method was applied for quantification of CO and HCOOH.

2.3. Electrochemical studies

The electrochemical measurements, namely linear sweep voltammetry (LSV), cyclic voltammetry (CV) and electrochemical impedance spectroscopy (EIS) were carried out using a potentiostat/galvanostat (SP-150, BioLogic Science Instruments, France). A conventional H-type cell with a three-electrode arrangement was used and the anode and cathode chambers were separated with a Nafion® 115 membrane. The Cu/NF and Cu-lignin/NF were used as working electrodes and platinum rod was used as a counter-electrode as the electrode chambers were separated by the Nafion® 115 membrane. Ideally, one should use graphite rod as the counter electrode but the mechanical stability is an issue with graphite rod. A CO_2 saturated 0.1 M Na_2SO_4 (50 mL, pH ≈ 6) solution was used as electrolyte. The Ag/AgCl (Sat. KCl) was used as a reference electrode with a potential of 0.551 Vs. RHE in CO_2 saturated 0.1 M Na_2SO_4 solution at a scan rate of 10 mV s^{-1}. N_2 saturated solutions were used for blank experiments. All electrochemical measurements were carried out at an ambient temperature (~22 °C) and pressure.

3. Results and discussion

3.1 Electrode preparation and characterization

Cu-lignin catalyst was deposited on NF surface by electrochemical deposition method. Based on preliminary experimental results, deposition time, temperature, stoichiometric ratio of Cu-lignin catalyst were selected for obtains ethanol as the product preferentially. Lignin is a structurally complex bio-derived polymer, containing oxygen functionalities that coordinate to Cu surfaces through phenolic moieties [31].

The SEM image of the bare NF (Fig. 2a), shows the well-known 3D network of porous NF structure which provides a high surface area, high flexibility and accumulated large space for electron/ion transport.

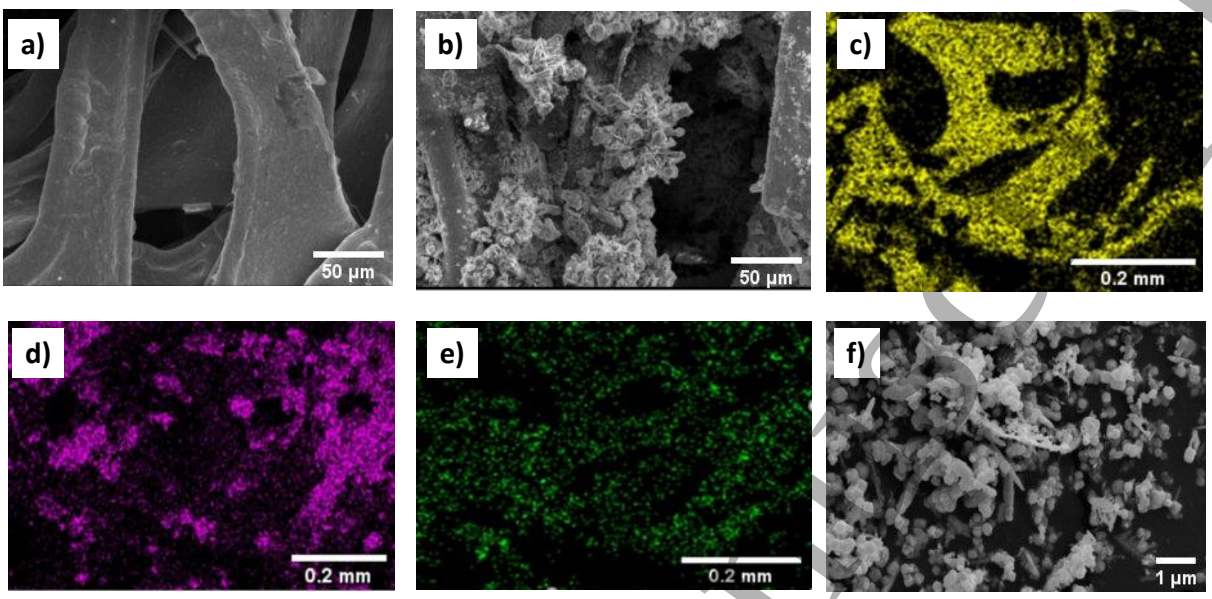

Fig. 2. Scanning electron microscope micrographs of (a) NF, (b) Cu-NF, (c-e) EDS elemental mapping images of Cu-NF showing the presence of Ni, Cu and O, and (f) SEM image of Cu without NF.

After deposition of Cu, it can be seen that the Cu particles are present on NF in uneven fashion and one can clearly see the irregular shapes of the particles, as shown in Fig. 2b. Elemental mapping by EDS confirmed the presence of Ni, Cu and O on the Cu-NF surface (Fig. 2c-e). The irregular shape of the Cu particles was also confirmed by the SEM image as seen in Fig. 2f.

The SEM image of the electrochemically deposited Cu-lignin on NF is shown in Fig. 3a. The Cu-lignin materials are uniformly distributed on the surface of 3D NF networks. A flake-like structure is observed on the surface of the NF, which was further confirmed by the SEM image shown in Fig. 3b. The detection of Cu, C, and O by the EDX mapping (Fig. 3c-f) confirms the presence of Cu-lignin catalyst on the NF layer.

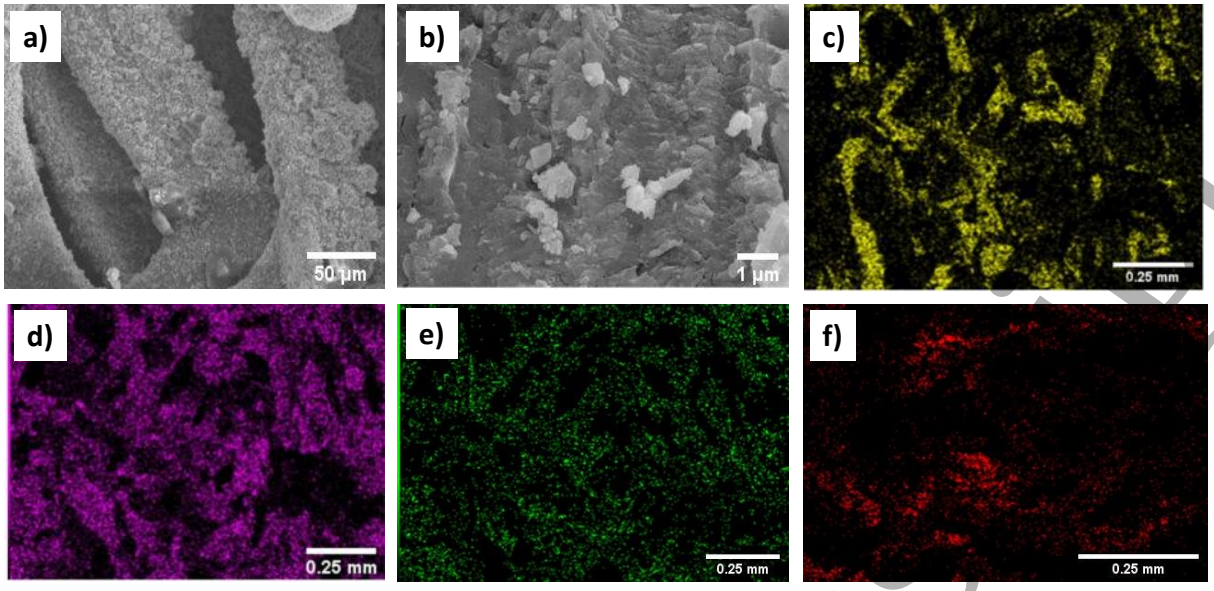

Fig. 3. Scanning electron microscope micrographs of (a) Cu-lignin-NF, (b) Cu-lignin (without NF). EDS elemental mapping images of Cu-lignin decorated NF showing the presence of (c) Ni, (d) Cu, (e) O and (f) C.

Fig. 4a shows the TEM image of Cu-lignin (scraped off from the NF substrate) and it can be seen that the Cu particles are interlinked by the carbon chain of the lignin. The HRTEM images of Cu-lignin (Fig. 4b-c) show many small Cu nanoparticles associated with carbon, and FFT (fast Fourier technique) pattern (Fig. 4d) shows the plane spacing 0.252 nm and 0.319 nm corresponding to the 100 and 110 planes of Cu(I). The FFT pattern in Fig. 4e indicates the presence of carbon microspheres. The selected area of electron diffraction (SAED) pattern in Fig. 4f, also confirmed the 100 and 110 planes of Cu(I). The CHNS analysis confirmed the presence of C (7.23 wt%) and H (16.5 wt%) in Cu-lignin-NF catalyst, which was the same as the amount in pristine lignin [33].

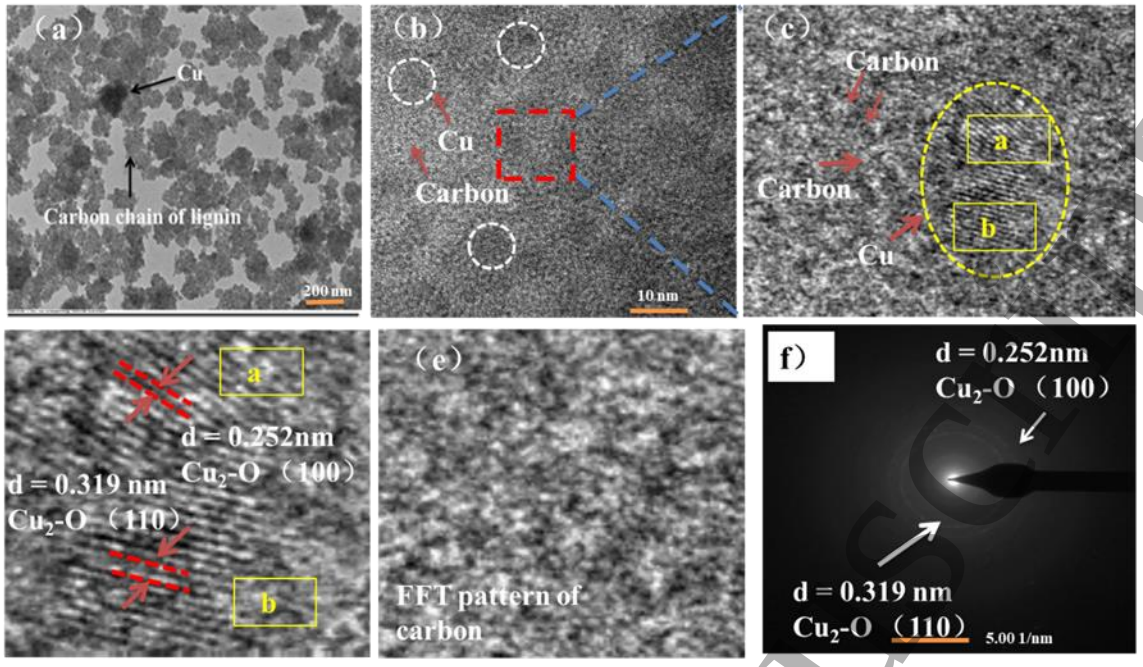

Fig. 4. (a) Transmission electron microscope images of Cu-lignin, (b-c) HRTEM image of Cu-lignin, (d) FFT pattern of Cu(e) FFT pattern carbon, and (f) SAED pattern of Cu.

The structure of lignin has been studied by numerous techniques including Raman, UV-Vis spectroscopies, FTIR, and XRD [32-38]. Fig. 5a. presents the Raman spectra (E Laser = 514 nm) of Cu, lignin and Cu-lignin powder materials. It should be noted that the Cu is not seen in the Raman spectra. The bands in the range of 1470–1200 cm^{-1} indicated the presence of different functional groups such as aliphatic-OH, aryl-OH and aryl-OCH_3 [33] which strongly interact with Cu(I) ions and form the Cu-lignin complex, consequently reducing the Raman spectra intensity. Also, the peak appearing at 1600 cm^{-1} indicates benzene-ring mode. However, the intensity of such peak also drops significantly in the presence of Cu(I), as it prevents the benzene-ring conjugation [34-35]. To further confirm the formation of Cu(I)-lignin complex, UV-Vis absorption spectra were recorded as shown in Fig. 5b. The spectra indicates that the absorption maxima of Cu-lignin shifted from 399.6 nm (for kraft lignin) to 394.5 nm which happens to be due to the interaction of Cu(I) with lignin moieties. So, the Cu clusters are converted to the Cu-lignin complex by application of negative potential.

The presence of organic functional groups of lignin and Cu-lignin are confirmed by FTIR as shown in Fig. 5c. A band that corresponds to C-H is observed at 2310 cm^{-1}. The broadband appearing at 3450 cm^{-1} corresponds to the asymmetric and symmetric stretching mode of O-H groups of alcohol or phenol. The band at 1635 cm^{-1} corresponds to C=C stretching mode of C=C at 1635 cm^{-1} represents the aromatic ring of the lignin. The bands in the range of 1500-

1000 cm^{-1} indicates the presence of different groups, namely, ether groups (C-O-C), C-H groups, C-C bonds, and C-O. These results are in good agreement with previously published work on lignin [36-37].

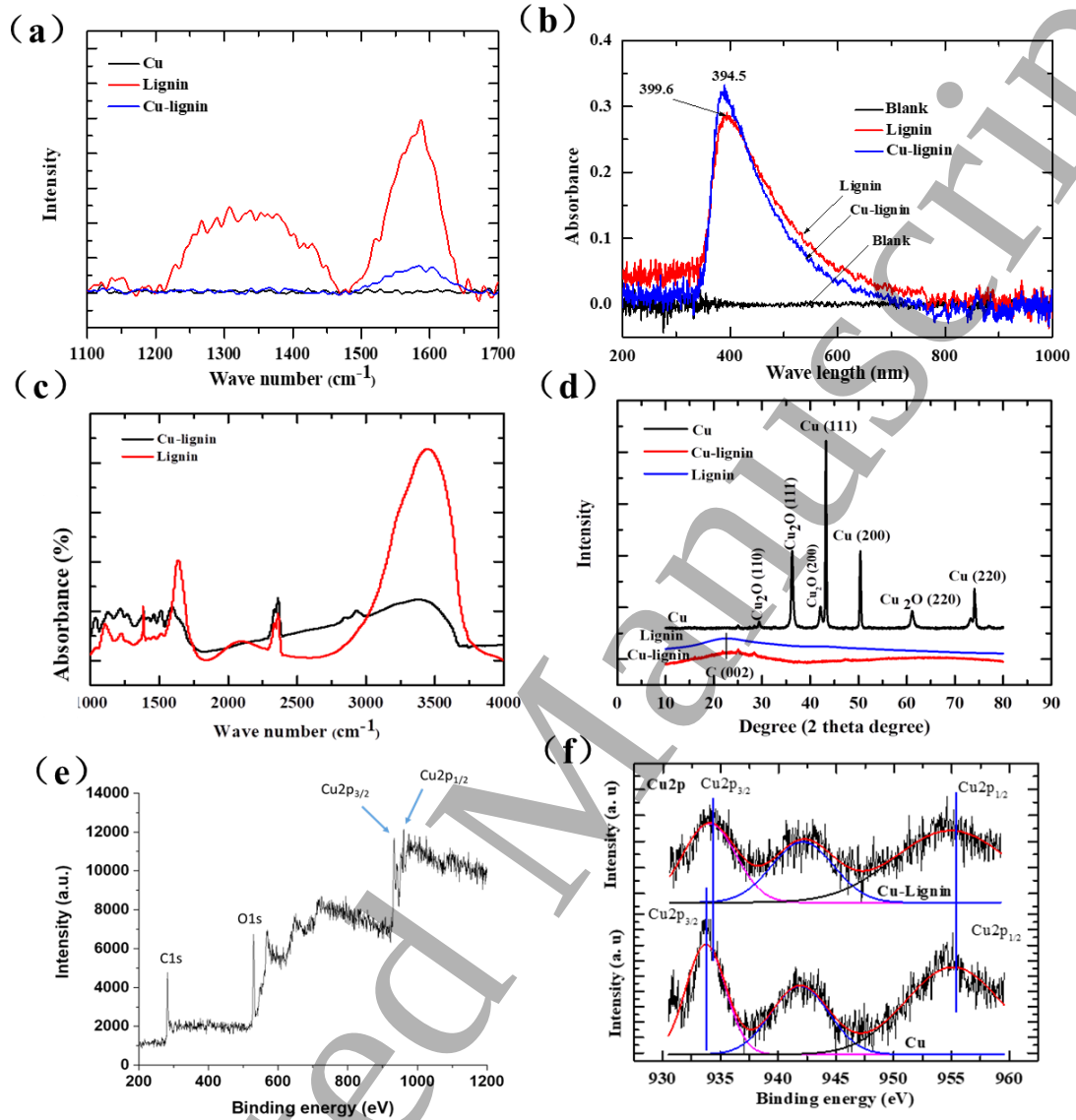

Fig. 5. Physical characterization of lignin, Cu, and Cu-lignin: (a) Raman spectroscopy (b) UV-Vis, (c) FT-IR, (d) XRD pattern, and (e) Full scale XPS spectra of Cu-lignin complex (f) XPS spectra of Cu2p (with fitting).

The FTIR spectra provide indirect information on the formation of Cu(II)-lignin complex. A significant drop in the intensity of the signals for -OH group is seen, confirming the presence of -OH attached to the positively charged Cu (II) ions via covalent bond formation. The Cu-lignin complex formation has been detected by a slight change in the maxima of absorption bands for functional groups of lignin in the FTIR spectra which is also related to the interaction

of those groups with Cu(II) ions. Fig. 5d presents the XRD patterns of lignin, Cu, and Cu-lignin samples. The measured peaks in XRD are found for Cu, corresponding to the Cu_2O (110), Cu_2O (111), Cu_2O (200), Cu (111), Cu (200), Cu_2O (220), Cu (220) crystallographic planes, indicating the presence of Cu and Cu_2O. In the XRD pattern of lignin, the strong peak generated at $2\theta = 22.6°$, indicates the presence of carbon plane (002) [36], which is consistent with the XRD pattern observed for Cu-lignin [36]. The XRD pattern for Cu-lignin is essentially a continuous in appreence with minor peaks which may be due to some impurities. The XRD data proved the amorphous nature of the Cu-lignin complex. The wide range of binding energy analysis indicates the presence of $C1_S$, $O1_S$ and $Cu2_P$ elements (Fig 5e). In XPS spectra (Fig. 5f), Cu-lignin-NF showed two main peaks assigned at 933 eV and 955 eV, which is associated with $Cu2p_{3/2}$ and $Cu2p_{1/2}$, respectively, and this indicates the presence of Cu(0) and Cu(I). In the case of Cu-lignin complex on NF, electron transfer can take place to the ligand at a 3d orbital of Cu, confirming that Cu species exist in Cu(I) form.

3.2. Electrochemical characterization

3.2.1 Cyclic voltammetry

Fig. 6 (a-c) displays the CVs of NF, Cu-NF, and Cu-lignin-NF. The Cu and Cu-lignin catalysts are well distributed on the macroporous NF layer thereby facilitating the accessibility of liquid reactant media through the open pore channels resulting in high electrochemically active surface area (ECSA). The ECSA of the electrode materials is an estimation from the non-faradaic capacitive current in double-layer charging of the electrode surface/electrolyte interface obtained from the CV at different scan rates. The estimation is performed for the working electrode within a small potential range of 0.0-0.6 V versus Ag/AgCl (sat. KCl) at the scan rate ranging from 10 to 90 mV s^{-1}. The relationship between the charging current (i at 0.3 V vs. Ag/AgCl, sat. KCl), scan rate (v) and the double-layer capacitance (C_{dl}) is given by: $i = vC_{dl}$. The C_{dl} can be obtained from the slope of the linear curves of i vs. v. As shown in Fig. 6d, the C_{dl} of NF, Cu-NF, and Cu-lignin-NF are estimated to be 0.5 mF cm^{-2}, 1 mF cm^{-2} and 8 mF cm^{-2}, respectively. Cu-lignin-NF has higher C_{dl} value and therefore a higher ECSA, which should have a positive impact on the electrocatalytic performance. The CV curves of NF, Cu-NF, and Cu-lignin-NF show a similar trend in oxidation and reduction current, whereas a minor change has been observed due to the iR resistance of the catalyst materials.

3.2.2 Linear sweep voltammetry

The electrochemical CO_2 reduction activity of the three different electrodes (NF, Cu-NF, and Cu-lignin-NF) was evaluated by determination of LSV in 0.1 M Na_2SO_4 solution saturated with argon and CO_2. As shown in Fig. 6e, the tested electrodes achieved a reasonable cathodic current at a potential of 0.5 V vs. RHE in an argon environment, which indicates the production of hydrogen at the applied voltage. A significant increase of cathodic current was observed in CO_2 atmosphere and the activity of the electrodes follow the trend: NF < Cu-NF < Cu-lignin-NF. The obtained CO_2 reduction current density for Cu-lignin-NF reached 22.5 mA cm^{-2} at -0.8 V vs. RHE which is much higher than Cu-NF (13.2 mA cm^{-2}) and NF (9.3 mA cm^{-2}). All LSV measurements were evaluated with respect to RHE. Although this imposes a possibility of change in the local pH, a one-time single measurement does not result in such a phenomenon. As discussed in the previsous sections, the different electrochemically active surface areas resulting from morphological difference in microscopic level could be the reason for such behavior.

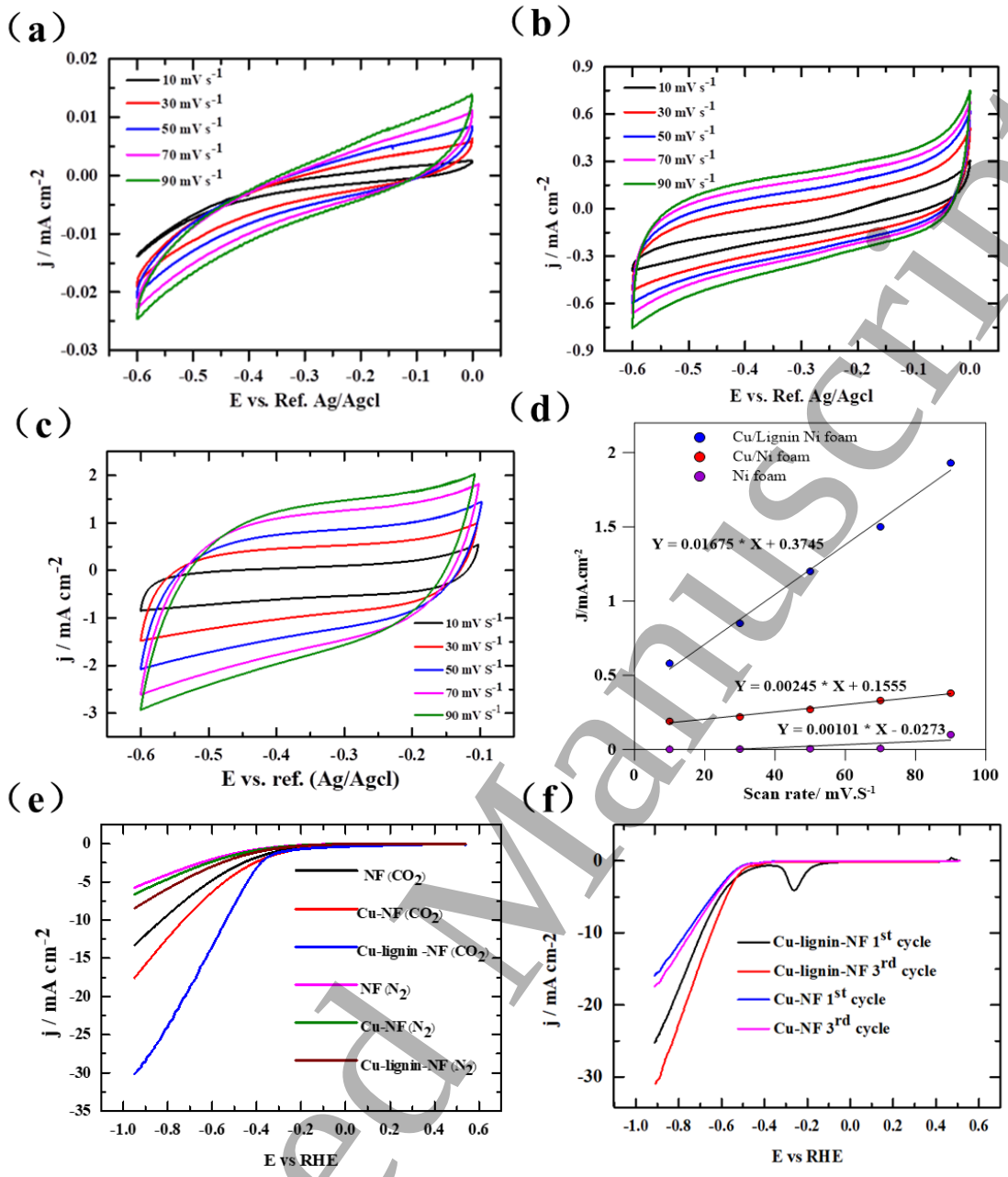

Fig. 6. Electrochemical determination of capacitance: cyclic voltammograms (CV) of (a) NF, (b) Cu-NF (c) Cu-lignin-NF in 0.1 M Na_2SO_4 in the non-Faradaic potential range of 0.00 V to -0.6 V at a scan rate of 10, 30, 50, 70 and 90 mV s^{-1}, respectively. (d) Average capacitive current for NF, Cu-NF, and Cu-lignin-NF at 0.30 V vs. Ag/AgCl (sat. KCl), and electrochemical CO_2 reduction on NF, Cu-NF, and Cu-lignin-NF surface, (e) Linear sweep voltammetry curves; (f) LSVs for electrochemically CO_2 reduction at different cycles in CO_2-saturated and N_2 saturated 0.1 M Na_2SO_4 solution.

It should be noted that all the LSVs are reported as an average of 3 to 5 cycles. For Cu-lignin-NF, a peak observed at 0.5 V (Fig. 6f) is associated with the change in the oxidation state of Cu (surface bounded Cu(II) to Cu(I)). However, this peak disappeared at the 3rd cycle but the current density increased which confirms the formation of Cu(I)-lignin complex and

change in the structure of lignin [37]. This marks the fact that the Cu(I) played a role as an active centre for electrochemical CO_2 reduction in the present study. Such type of behavior is not observed for Cu-NF where Cu is present at an oxidation state of Cu (I) as confirmed by XRD of Cu_2O. Moreover, in N_2 atmosphere, the transition of Cu(II) to Cu(I) was not observed which means that the intermediates of CO_2 reduction process was influenced by the change in oxidation state of Cu. The higher catalytic activity of Cu-lignin-NF originated from the strong interaction between Cu-lignin and NF along with the uniform distribution of the Cu-lignin catalysts on the conductive NF surface. The reduction of Cu metal center and exposes active catalytic sites facilitating the multiple proton-coupled electron transfer and ion transport throughout the layer to achieve a higher current density. Moreover, catalytic products would depend on the the metal centre as well as catalyst support. Since Cu-lignin is deposited on NF by an electrochemical method, it minimizes the catalyst aggregation and exposes the higher active sites compared to other methods, e.g. dip coating, spin coating, and spraying. Overall, the LSV analysis shows excellent cathodic CO_2 reduction current (32 mA cm^{-2}) at the low over-potential region (-0.6 to -0.9) for Cu-lignin-NF catalyst.

4.3 Products analysis and faradaic efficiency

In the present study, electrochemical CO_2 reduction products distribution and corresponding FE at different potentials are presented in Fig. 7a-d and Fig. S1 (SI supporting information). As indicated, multiple ECR products were formed, such as CO, HCOOH, C_2H_5OH.

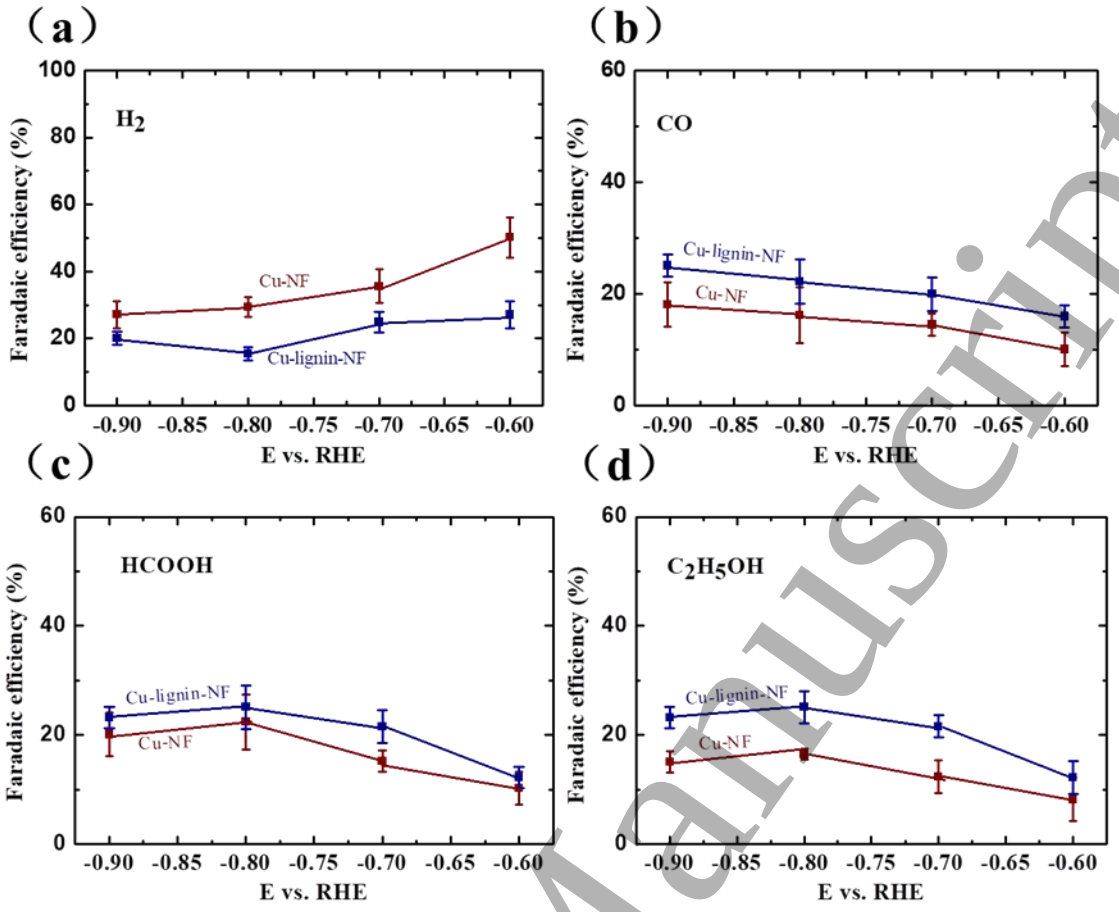

Fig. 7. Faradaic efficiency of CO_2 reduction on Cu-NF and Cu-lignin-NF at different potential: (a) H_2, (b) CO, (c) HCOOH, and (d) C_2H_5OH.

In the potential range -0.6 to -0.9 V, FE of HCOOH increases on Cu-NF and Cu-lignin-NF electrode at more negative potentials and reach it maximum at -0.8 V *vs*. RHE (Fig. 7c). The FE for ethanol increases with the increase in potential for both Cu-NF and Cu-lignin-NF electrode. The maximum FE is achieved at -0.8 V *vs*. RHE, and then decreases at a higher potential, due to the dominance of hydrogen production. The FE obtained for Cu-NF electrode reaches 16.5 % at -0.8 V *vs*. RHE, whereas the FE for Cu-lignin-NF reaches 23.2 %. Cu-lignin-NF electrode shows similar FE of ethanol production compared to most of the recently studied Cu-based electrocatalysts as shown in Table 1. In the case of CO, the FE continuously increases to a maximum value of 18.1 % for Cu-NF and 23.5 % for Cu-lignin-NF at a potential of -0.9 V RHE (Fig. 7b). The Cu-lignin-NF and Cu-NF electrodes showed the maximum FE for H_2 generation of 26.5 % and 50.2 % at -0.6 *V vs*. SHE, respectively (Fig. 7a). On bare Ni foam, the FE of H_2 was very high (92.5 %), and CO_2 reduction products are not favorable (not shown). Ni catalytic reaction is poor in reproducibility because of the formation of nickel-hydride, which can prevent further electrocatalytic reaction. However, the catalytic

layer on Ni foam can mitigate the above mention problem [43]. Moreover, the Cu-lignin-NF and Cu-NF electrodes exhibited much higher FE for CO_2 reduction to C_2H_5OH than CO generation and Cu-lignin-NF exhibited higher FE for all products compared to the other tested catalysts (Fig. 7d).

Table 1. Comparison of ethanol production (Bulk electrolysis) Faradaic efficiency with recently published literature.

Electrode	**Electrolyte**	**Faradaic efficiency (ethanol), voltage (V vs. RHE)**	**Ref.**
Cu-lignin-NF	0.1 M Na_2SO_4	23.2 %,-0.8	This work
Cu-NF	0.1 M Na_2SO_4	16.5 %,-0.8	This work
Cu/CNS	0.1 M $KHCO_3$	63 %,−1.2	[38]
Cu mesh	0.5 M $KHCO_3$	13 %, -1	[39]
3D CuO	0.1 M $KHCO_3$	13 %, -0.816	[40]
Cu/TiO_2	0.2 M KI	27.4 %, -1.45	[41]
Graphene/Cu_2O	0.5 M $NaHCO_3$	9.93 %, -0.9	[42]
Cu_4Zn	0.1 M $KHCO_3$	29.1 %, 1.05	[27]

4.4 Electrochemical impedance spectroscopy (EIS)

Fig. S2a presents the Nyquist plots of the NF, Cu-NF, and Cu-lignin-NF electrodes determined in CO_2-saturated 0.1 M Na_2SO_4 solutions at -0.8 vs. RHE in the frequency range 10 kHz to 10 Hz. The Cu-lignin-NF electrode shows very small semi-circle, which indicates lower charge transfer resistance and a fast CO_2 reduction reaction kinetics. The results indicates that the charge transfer resistance (R_{ct}) value gradually decreases in the following order: Ni-NF > Cu-NF > Cu-lignin-NF.

Stability tests were conducted through chronoamperometric method with continuous CO_2 bubbling in selected potential range (-0.6, -0.7, -0.8 and -0.9 V vs. RHE) (Fig. S2b). The current was measured at each selected potentials which remained constant for all the electrodes (NF, Cu-NF, and Cu-lignin-NF) during 6 h (Fig. S2b). After 24 h of CO_2 reduction process, the Cu-NF electrode displayed a more deterioration compared to Cu-lignin-NF. The deterioration could possibly be due to the dissolution of the Nafion binder, which is associated with the catalyst degradation. Our previous study [17] conclusively found out that Cu catalysts degrade from carbon paper electrode under similar condition. In the case of Cu-lignin-NF catalyst, the lignin might interlink with NF by its carbon chain and functional groups which prevents the loss of the catalyst from the NF surface. Moreover, only small amount of Cu was

detected in the electrolyte solution (0.229 ppb when using Cu-NF and 0.208 ppb when using Cu-lignin-NF) as revealed by the ICP-MS carried after 24 h of CO_2 reduction operation. Futhermore, the SEM of the electrode before and after CO_2 reduction, shows that there is no significant change has been observed (Fig. S2 c and d).

4. Conclusions:

Electrochemical reduction of CO_2 to ethanol is demonstrated on a stable Cu-lignin decorated NF electrode. A facile and reproducible electro-deposition method has been used for the fabrication of Cu and Cu-lignin coated NF catalyst electrodes for electrochemical CO_2 reduction. Overall, the Cu-lignin decorated NF electrode showed the most promising electrocatalytic activity and selectivity towards ethanol production with a faradaic efficiency reaching up to 23.2 % at -0.8 V vs. RHE and current density of 22.5 mA cm^{-2}. This observation is attributed to the unique structure of Cu-lignin-NF, which incurs more active surface area to the electrode and the change in the oxidation state of the Cu center with lignin as unified by the charge balance. Moreover, the Cu-lignin-NF was found to be sufficiently durable for long-term ethanol production, however, withfurther research required for a more selective and durable CO_2 electroreduction by tuning the structure of such catalysts based on metal-organic molecular complexes.

Corresponding Author

Email: sbasu@immt.res.in (Prof. Suddhasatwa Basu),

tel: +91(0674) 2567126,

Notes

The authors declare no competing financial interest.

Acknowledgment:

The financial support of this research by the SERB (NPDF) India through the project No. PDF/ 2017/001375 and the Marie Sklodowska-Curie grant agreement no. 713683 (H.C. Ørsted COFUND program) is gratefully acknowledged.

References:

1. J. D. Shakun, P. U. Clark, F. He, A. S. Marcott, C. A. Mix, Z. Liu, O. B. Bliesner, A. Schmittner, E. Bard, Global Warming Preceded by Increasing Carbon Dioxide Concentrations During the Last Deglaciation, Nature 484 (2012) 49−54.
2. R. A. Tufa, D. Chanda, M. Ma, D. Aili, T. B. Demissie, J. Vaes, Q. Li, S. Liu, D. Pant, Towards Highly Efficient Electrochemical CO2 Reduction: Cell designs, Membranes and Electrocatalysts, Applied energy, 277 (2020) 115557.
3. A. T. Najafabadi, CO_2 Chemical Conversion to Useful Products: an Engineering Insight to the Latest Advances Toward Sustainability, Int. J. Energy Res. 37 (2013) 485−499.
4. H. Jiang,, Y. Zhao, L. Wang, Y. Kong, F. Li, P. Li, Electrochemical CO_2 reduction to formate on Tin cathode: Influence of anode materials, Journal of CO_2 Utilization, 26 (2018) 408– 414.
5. H. Xiang, S. Rasul, K. Scott, J. Portoles, P. Cumpson, E. H.Yu, Enhanced selectivity of carbonaceous products from electrochemical reduction of CO_2 in aqueous media, Journal of CO_2 Utilization, 30 (2019) 214– 221.
6. T. Pardal, S. Messias, M. Sousa, A. S. ReisMachado, C. M.Rangel, D. Nunes, J. V. Pinto, R.Martins, M. N. Ponte, Syngas production by electrochemical CO_2 reduction in an ionic liquid based-electrolyte, Journal of CO_2 Utilization, 18 (2017) 62– 72.
7. T. Moller, W. Ju, A. bagger, X. wang, F. Luo, T. N. Thanh, A. S. Varela, J. Rossmeisl, P. Strasser, Efficient CO_2 to CO Electrolysis on Solid Ni-N-C Catalysts at Industrial Current Densities, Energy Environ. Sci., 12 (2019) 640-647.
8. H. Y. Kim, S. H. Joo, Recent advances in nanostructured intermetallic electrocatalysts for renewable energy conversion reactions. J. Mater. Chem. A, 8 (2020) 8195-8217.
9. N. Furuya, K. Matsui, Electroreduction of Carbon Dioxide on Gas-Diffusion Electrodes Modified by Metal Phthalocyanines, J. Electroanal. Chem. Interfacial Electrochem. 271 (1989) 181-191.
10. V. T. Magdesieva, T. Yamamoto, A. D. Tryk, A. Fujishima, A. Electrochemical Reduction of CO_2 with Transition Metal Phthalocyanine and Porphyrin Complexes Supported on Activated Carbon Fibers, J. Electrochem. Soc. 149 (2002) D89-D95.

11. S. Kapusta, N. Hackerman, Carbon Dioxide Reduction at a Metal Phthalocyanine Catalyzed Carbon Electrode, J. Electrochem. Soc. 131 (1984) 1511-1514.
12. N. Sonoyama, M. Kirii, T. Sakata, Electrochemical Reduction of CO_2 at Metal-Porphyrin Supported Gas Diffusion Electrodes Under High Pressure CO, Electrochem. Commun. 1 (1999) 213-216.
13. J. Shen, R. Kortlever, R. Kas, Y. Y. Birdja, O. Diaz-Morales, Y. Kwon, I. Ledezma-Yanez, P. J. K. Schouten, G. Mul, M. T. M. Koper, Electrocatalytic Reduction of Carbon Dioxide to Carbon Monoxide and Methane at an Immobilized Cobalt Protoporphyrin, Nat. Commun. 6 (2015) 8177-8194.
14. S. Popovic, M. Smiljanic, P. Javanovic, J. Vavra, R. Buonsanti, N. Hodnik, Stability and Degradation Mechanisms of Cupper-based Catalysts for Electrochemical CO_2 Reduction, Angewandte Chemie International Edition, 59 (2020) 14736-14746.
15. D. Voiry, H. S. Shin, K. P. Loh, M. Chhowalla, Low-dimensional Catalysts for Hydrogen Evolution and CO_2 Reduction, Nature Reviews Chemistry 8109,2 (2018) 0105.
16. S. Ma, M. Sadakiyo, R. Luo, M. Heima, M. Yamauchi, A. J. P. Kenis, One-step Electrosynthesis of Ethylene and Ethanol from CO_2 in an Alkaline Electrolyzer, J. Power Sources 301 (2016) 219−228.
17. G. Garg. S. Basu, Studies on Degradation of Copper Nano Particles in Cathode for CO_2 Electrolysis to Organic Compounds, Electrochimica Acta 177 (2015) 359-365.
18. D. Ren, Y. Deng, D. A. Handoko, S. C. Chen, S. Malkhandi, S. B. Yeo, Selective Electrochemical Reduction of Carbon Dioxide to Ethylene and Ethanol on Copper(I) Oxide Catalysts, ACS Catal. 5 (2015) 2814−2821.
19. A. D. Handoko,W. C. Ong, Y. Huang, G. Z. Lee, L. Lin, B. G. Panetti, S. B. Yeo, Mechanistic Insights into the Selective Electroreduction of Carbon Dioxide to Ethylene on Cu_2O-Derived Copper Catalysts, J. Phys. Chem. C 120 (2016) 20058−20067.
20. R. Kas, R. Kortlever, A. Milbrat, M. Koper, G. Mul, G Baltrusaitis, J. Electrochemical CO_2 Reduction on Cu_2O-Derived Copper Nanoparticles: Controlling the Catalytic Selectivity of Hydrocarbons, Phys. Chem. Chem. Phys. 16 (2014) 12194−12201.
21. S. Min, X. Yang, A. Y. Lu, C. C. Tseng, M. N. Hedhili, L. J. Li, K. W. Huang, Low Overpotential and High Current CO_2 Reduction with Surface Reconstructed Cu foam Electrodes, Nano Energy 27 (2016) 121-129.

22. H. Yano, T. Tanaka, M. Nakayama, K. Ogura, Selective Electrochemical Reduction of CO_2 to Ethylene at a Three-Phase Interface on Copper (I) Halide-Confined Cu-Mesh Electrodes in Acidic Solutions of Potassium Halides, J. Electroanal. Chem. 565 (2004) 565, 287−293.
23. P. K. Kuhl, R. E. Cave, N. D. Abram, F. T. Jaramillo, New Insights into the Electrochemical Reduction of Carbon Dioxide on Metallic Copper Surfaces, Energy Environ. Sci. 5 (2012) 7050−7059.
24. S. C. Chen, D. A. Handoko, H. J. Wan, L. Ma, D. Ren, S. B. Yeo, Stable and Selective Electrochemical Reduction of Carbon Dioxide to Ethylene on Copper Mesocrystals. Catal. Sci. Technol. 5 (2015) 161−168.
25. Y. Hori, H. Wakebe, T. Tsukamoto, O. Koga, Electrocatalytic Process of CO Selectivity in Electrochemical Reduction of CO_2 at Metal Electrodes in Aqueous Media. Electrochim, Acta 39 (1994) 1833−1839.
26. Y. Liu, Y. Zhang, K. Cheng, X. Quan, X. Fan, Y. Su, S. Chen, H. Zhao, Y. Zhang, H. Yu, M. R. Hoffmann, Selective Electrochemical Reduction of Carbon Dioxide to Ethanol on a Boron and Nitrogen-Co-doped Nanodiamond, Angew. Chem. Int. Ed. 56 (2017) 15607 –15611.
27. D. Ren, S. H. Ang, B. S. Yeo, Tuning the Selectivity of Carbon Dioxide Electroreduction Toward Ethanol on Oxide-Derived Cu_xZn Catalysts, ACS Catal. 6 (2016) 8239−8247.
28. Z. Weng, J. Jiang, Y. Wu, Z. Wu, X. Guo, K. L. Materna, W. Liu, V. S. Batista, G. W. Brudvig, H. Wang, Electrochemical CO_2 Reduction to Hydrocarbons on a Heterogeneous Molecular Cu Catalyst in Aqueous Solution, J. Am. Chem. Soc. 138 (2016) 8076−8079.
29. P. K. Kuhl, T. Hatsukade, R. E. Cave, N. D. Abram, J. Kibsgaard, F. T. Jaramillo, Electrocatalytic Conversion of Carbon Dioxide to Methane and Methanol on Transition Metal Surfaces, J. Am. Chem. Soc. 136 (2014) 14107-14113.
30. D. A. Torelli, A. Francis, J. C. Crompton, A. Javier, R. Jonathan, J. R. Thompson, B. S. Brunschwig, M. P. Soriaga, N. S. Lewis, Nickel–Gallium-Catalyzed Electrochemical Reduction of CO_2 to Highly Reduced Products at Low Overpotentials, ACS Catal. 6 (2016) 2100−2104.

31. C. W. Owens, G. S. Oporto, B. C. G. Söderberg, K. E. Lambson, Lignocellulosic Micro and Nanomaterials as Copper Frames for the Evaluation of the Copper(I)-Catalyzed Azide-Alkyne Cycloaddition, Journal of Nanomaterials 2017, 6.
32. E. D. Bartzoka, H. Lange, K. Thiel, C. Crestini, Coordination Complexes and One-Step Assembly of Lignin for Versatile Nanocapsule Engineering, ACS Sustainable Chem. Eng. 4 (2016) 5194−5203.
33. U. P. Agarwal, J. D. McSweeny, S. A. Ralph, FT–Raman Investigation of Milled-Wood Lignins: Softwood, Hardwood, and Chemically Modified Black Spruce Lignins, Journal of Wood Chemistry and Technology, 31 (2011) 324–344.
34. M. Wysokowski, L. Klapiszewski, D. Moszyński, P. Bartczak, T. Szatkowski, I. Majchrzak, K. S. Stefańska, V. V. Bezhenov, T. Jesionowski, Modification of Chitin with Kraft Lignin and Development of New Biosorbents for Removal of Cadmium(II) and Nickel(II) Ions, Mar. Drugs, 12 (2014) 2245-2268.
35. K. Bula, L. Klapiszewski, T. Jesionowski, A Novel Functional Silica/Lignin Hybrid material as a Potential BioBased Polypropylene Filler, Polym. Compos., 36 (2015) 913-922.
36. X. Wang, X. Cui, L. Zhang. L. Preparation and Characterization of Lignin-Containing Nanofibrillar Cellulose, Procedia Environmental Sciences 2012 , 16, 125–130.
37. Q. Li, W. Zhu, J. Fu, H. Zhang, G. Wu, S. Sun, Controlled Assembly of Cu Nanoparticles on Pyridinic-N Rich Graphene for Electrochemical Reduction of CO_2 to Ethylene, Nano Energy 24 (2016) 1-9.
38. Y. Song, R. Peng, D. K. Hensley, P. V. Bonnesen, L. Liang, Z. Wu, H. M. Meyer, M. Chi, C. Ma, B. G. Sumpter, A. J. Rondinone, High Selectivity Electrochemical Conversion of CO_2 to Ethanol Using a Copper Nanoparticle/N Doped Graphene Electrode, Chem. Select 1 (2016) 6055-6061.
39. M. Rahaman, A. Dutta, A. Zanetti, P. Broekmann, Electrochemical Reduction of CO_2 into Multicarbon Alcohols on Activated Cu Mesh Catalysts: An Identical Location (IL) Study, ACS Catal. 7 (2017) 7946-7956.
40. F. S. Ke, X. C. Liu, J. Wu, P. P. Sharma, J. Z. Y. Zhou, D. X. Qiao, X. Zhou. Selective Formation of C_2 Products from the Electrochemical Conversion of CO_2 On CuO-Derived Copper Electrodes Comprised of Nanoporous Ribbon Arrays, Catalysis Today 288 (2017) 18-23.

41. J. Yuan, L. Liu, R. R. Guo, S. Zeng, H. Wang, X. Lu, Electroreduction of CO_2 into Ethanol over an Active Catalyst: Copper Supported on Titania, J.Catalysts 7 (2017) 220-230.
42. R. A. Geioushy, M. Khaled, A. S. Hakeem, K. Alhooshani, C. Basheer, High Efficiency Graphene/Cu_2O Electrode for the Electrochemical Reduction of Carbon Dioxide to Ethanol, J. Electroanal. Chem. 785 (2017) 138-143.
43. D. Chanda, J. Hnat, A. S. Dobrota, I. A. Pasti, M. Paidar, K. Bouzek, The Effect of Surface Modification by Reduced Graphene Oxide on the Electrocatalytic Activity of Nickel Towards the Hydrogen Evolution Reaction, Phys.Chem.Chem.Phys., 17 (2015) 26864-26874.